

Emergent Random Spin Singlets in Disordered Spin-1/2 perovskite $\text{BaCu}_{1/3}\text{Ta}_{2/3}\text{O}_3$

Sagar Mahapatra,¹ Francesco De Angelis,² Dibyata Rout,¹ Priyanshi Tiwari,³ Martin Etter,⁴ Edmund Welter,⁴ M. P. Saravanan,³ Rajeev Rawat,³ Satoshi Nishimoto,⁵ Carlo Meneghini,² and Surjeet Singh^{1,5,*}

¹Department of Physics, Indian Institute of Science Education and Research, Pune 411008, Maharashtra, India

²Dipartimento di Scienze, Università Roma Tre, I-00146 Roma, Italy

³UGC-DAE Consortium for Scientific Research, University Campus, Khandwa Road, Indore 452 001, India

⁴Deutsches Elektronen-Synchrotron (DESY), Notkestraße 85, 22607 Hamburg, Germany

⁵IFW Dresden, Helmholtzstr. 20, 01069 Dresden, Germany

We investigate the disordered perovskite $\text{BaCu}_{1/3}\text{Ta}_{2/3}\text{O}_3$, where Cu (spin-1/2) and Ta randomly occupy a pseudo-cubic lattice. Synchrotron X-ray diffraction and X-ray absorption spectroscopy establish the local nature of the disorder, revealing the presence of structurally constrained magnetic exchange paths. No magnetic ordering or spin freezing is observed down to 0.1 K. The low-temperature magnetic and thermodynamic behavior is captured by a broad but non-singular distribution $P(J)$ of exchange couplings J . These results open the possibility of realizing a disordered quantum ground state where the exchange randomness is broad yet intrinsically bounded, departing from the conventional infinite-randomness fixed point driven random-single phase.

Quenched disorder in quantum spin systems has been a topic of considerable interest. In one-dimensional Heisenberg antiferromagnetic spin-1/2 model, the quenched disorder results in a novel Random Singlet (RS) ground state, arising from an infinite-randomness fixed point in the real-space renormalization-group flow. The RS phase comprises of spin dimers at arbitrarily large separations, with the exchange couplings J described by a broad, scale-free probability distribution $P(J)$ [1–3].

Importantly, the RS phase has also been shown to emerge in highly frustrated quantum magnets with quenched disorder [4]. In the absence of disorder, these systems exhibit novel quantum spin liquid ground states. However, when disorder is included, the RS phase emerge as a competing ground state. The effective coupling between the spins forming the RS phase follows a scale-free, power-law distribution $P(J) \sim J^{-\gamma}$, leading to thermodynamic quantities diverging at low-temperatures as: $\chi \propto T^{-\gamma}$, $c_{\text{mag}} \propto T^{1-\gamma}$, where χ and c_{mag} are magnetic susceptibility and magnetic specific heat, respectively.

An important consequence of effective $J^{-\gamma}$ distribution is the emergence of scale-invariant behavior, manifested by the collapse of $MT^{\gamma-1}$ versus μ_0H/T , and $(\mu_0H)^\gamma c_{\text{mag}}/T$ versus T/μ_0H plots over a wide range of temperatures and magnetic fields (henceforth referred to as $M[H, T]$ - and $c[H, T]$ -scaling, respectively). Such scaling behavior has been demonstrated for various frustrated spin systems with quenched disorder, including $\text{LiZn}_2\text{Mo}_3\text{O}_8$ [5], $\text{ZnCu}_3(\text{OH})_6\text{Cl}_2$ [6], YbMgGaO_4 [7], YbZnGaO_4 [8], Y_2CuTiO_6 [9], $\text{Sr}_2\text{IrO}_{6-\delta}$ [10], and Ba_2YMoO_6 [11].

Recently, the RS phase has been proposed for the perovskite spin-1/2 cuprates, $\text{SrCu}_{1/3}M_{2/3}\text{O}_3$ ($M = \text{Ta}$ or Nb) [12, 13]. In these perovskites the B-site forms an pseudo-cubic lattice ($c/a \approx 1$), randomly occupied by magnetic Cu and non-magnetic Ta(Nb). These com-

pounds do not exhibit magnetic long-range ordering or spin freezing down to the lowest temperatures. Their low-temperature magnetic and thermodynamic properties have been argued to be compliant with the RS ground state.

The 33% spin-1/2 occupancy ($\text{Cu}/M \equiv 1/2$), which exceeds the 31% percolation threshold of a cubic lattice, raises question about the apparent absence of large Cu-connected clusters that typically favor tendency towards magnetic ordering or spin freezing phase [14]. This naturally raises question about the precise nature of Cu- M disorder in these perovskites? In particular, what makes this disorder sufficiently strong to generate $P(J) \propto J^{-\gamma}$ distribution? Here, we attempt to understand these questions and, in conjunction, we also closely examine the nature of the ground state in these materials: i.e., given the non-frustrated lattice and high concentration of magnetic spins, what makes the low-energy effective distribution vary as $J^{-\gamma}$?

To address these questions, here we examine $\text{BaCu}_{1/3}\text{Ta}_{2/3}\text{O}_3$ (BCTO). True to its sister compounds, no long- or short-ranged magnetic ordering is detected in BCTO down to the lowest measured temperature of 0.1 K. The low-temperatures specific heat is characterized by a broad Schottky anomaly with associated entropy saturating around $0.4R\ln 2$, indicating that a large fraction of the spins remain dynamic down to 0.1 K. $\chi(T)$ exhibits a power-law-like divergence at low temperatures for $\gamma \approx 0.67$. The $M(H)$ plots in the same temperature range show $M[H, T]$ -scaling. However, the $c[H, T]$ -scaling or $c_{\text{mag}} \propto T^{1-\gamma}$ are not observed for any non-zero γ (specifically $\gamma = 0.67$), suggesting that the magnetic ground state is more complex than the RS phase.

To gain understanding of the BCTO atomic structure, we used synchrotron-based powder X-ray diffraction (XRD) and X-ray absorption spectroscopy (XAS) to probe the long range (crystallographic) and local atomic structure, respectively. We show that Cu and Ta distribution is statistically homogeneous throughout the lattice, without evidence for macroscopic phase separa-

* surjeet.singh@iiserpune.ac.in

tion. However, the local structure reveals a prevalence of hetero-atomic Cu-O-Ta pairs with roughly equal numbers of Cu and Ta around the Ta absorber ($Ta-Cu/Ta \approx 2.9/3.1$), but a Ta rich environment around the Cu absorber ($Cu-Cu/Ta \approx 0.4/5.6$), leading to magnetic exchange paths such as Cu-O-Ta-O-Cu, Cu-O-Ta-O-Ta-O-Cu, and so on. The EXAFS results ensure the occasional presence of a Cu-O-Cu type exchange, while the roughly 50% probability of finding Cu or Ta around Ta ensures that the average Cu–Cu separation does not grow arbitrarily, thus preventing $P(J)$ from becoming singular as $J \rightarrow 0$.

We thus analyzed the experimental data using a data-driven distributed exchange dimer model, which yields a very broad $P(J)$; however, unlike a scale-invariant $J^{-\gamma}$ form, the derived $P(J)$ is non-singular, featuring a broad peak centered around 4 K with additional shoulder-like features near 70 K and 0.1 K. This form of $P(J)$, characterized by a long but non-diverging low- J tail, is consistent with the Cu-Ta disorder revealed by EXAFS, allowing a unified description of the temperature and field dependence of susceptibility and specific heat.

The BCTO sample was synthesized by a conventional solid-state reaction at 1100°C. It adopts an ABO_3 -type tetragonal perovskite structure, comprising a pseudo-cubic unit cell whose center is occupied by $A = Ba$ and corners randomly by $B = Cu$ and Ta in 1 : 2 ratio, with Cu/Ta–O–Cu/Ta bonds align along the edges [Fig. 1(b)]. Detailed synchrotron XRD analysis reveals two closely related tetragonal phases, $P4mm$ and $P4/mmm$. The main crystallographic difference between the two structures is a very slight off-centering of the B-site in the $P4mm$ phase, which primarily contributes to further broadening of J , as will become clear in the subsequent discussion. For details of structural refinement, refer to the Supplementary Material [15].

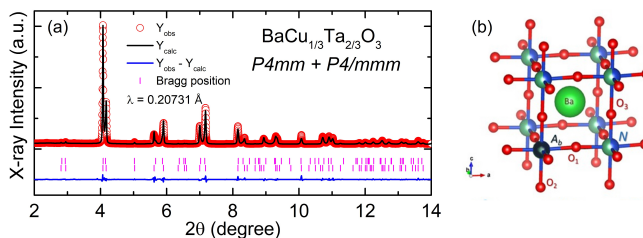


FIG. 1. (a) The Rietveld refinement of X-ray powder diffraction patterns of BCTO, (b) a schematic of the unit cell of the BCTO crystal structure. Here, A_b and N are the absorbing atom and the nearest-neighbour atom, respectively, as discussed in the XAS (see text).

EXAFS results are summarized in Fig. 2. The normalized Cu-K and Ta-L_{III} edge spectra in the XANES region (Fig. 2) confirm Ta^{5+} and Cu^{2+} charge states. The Ta-L_{III} edge exhibits an intense white-line ascribed to dipole allowed photoelectron excitations from 2p core to empty 5d states. The bimodal shape of the white-line can be

attributed to the $e_g - t_{2g}$ splitting of about 4 eV in agreement with O_h coordination symmetry. [16] The tiny and broad pre-edge shoulder of Cu-K suggests Jahn-Teller distorted octahedral geometry. The k^2 -weighted experimental EXAFS spectra, $k^2\chi^{\text{exp}}$, and the corresponding best-fit curves at the Cu, and Ta edges are shown in Fig. 2, together with the moduli of the Fourier transforms $|\text{FT}|$ of both k^2 -weighted experimental data and best-fit curves. The $|\text{FT}|$ representation provides a more intuitive view of the coordination shells around the absorber, despite distortions introduced by phase-shift effects, amplitude modulation, and interference between different scattering contributions [17]. The main peak around 1.6 Å in Fig. 2 (squeezed by phase shift effect) is ascribed to the oxygen coordination shell around Cu or Ta absorbers. The complex features between 2.5 Å and 4.5 Å account for contributions coming from single-scattering (SS), and multiple-scattering (MS) paths necessitated by the nearly collinear geometry of Cu-O-Ta bonds (see Fig. 1). The main results are summarized in Table I. For details of EXAFS analysis, see Supplementary Material [15].

TABLE I. Results of the EXAFS data refinement at the Cu K and Ta L_{III} edges, compared with crystallographic distances based on XRD Rietveld analysis. (See Supplementary Material for details [15].

	Cu K-Edge			Ta L _{III} -Edge			
	R _{XRD}	N	R	$\sigma^2 \times 10^2$ (Å ²)	N	R	$\sigma^2 \times 10^2$ (Å ²)
O ₁	2.022	4	2.03(1)	0.87(4)	6	1.98(1)	0.89(3)
O ₂	2.095	2	2.32(1)	0.87			
Ba	3.545	8	3.55(2)	1.3(2)	8	3.55(1)	0.95(8)
Ta(SS)	4.1	5.6(3)	4.05	0.67	3.1(3)	3.93(3)	1.9(3)
Cu(SS)	4.1	0.4	4.19(2)	2.2	2.9	4.05(3)	0.67(5)

The EXAFS analysis (Table I) shows that the local coordination geometries of the CuO_6 and TaO_6 octahedra deviate significantly from the average crystallographic structure one obtains using XRD [18]. In particular, the CuO_6 octahedra appear strongly Jahn-Teller distorted, with four shorter Cu–O₁ bonds ($R_{CuO_1} \simeq 2.03$ Å) and two longer Cu–O₂ bonds ($R_{CuO_2} \simeq 2.30$ Å). In contrast, a single oxygen coordination shell is found around Ta ($R_{TaO} \simeq 1.98$ Å). The averagely longer Cu–O distances are consistent with the larger ionic radius of Cu^{2+} (0.73 Å) compared with Ta^{5+} (0.64 Å). More importantly, EXAFS analysis makes it possible to obtain information on the chemical ordering in a binary alloy [19, 20], as described in detail in the Appendix section. As depicted in Table I, each Ta-absorber has roughly equal number of Ta and Cu atoms around it ($N_{Ta-Ta/Cu} \approx 3.1/2.9$). In contrast, each Cu absorber is surrounded by significantly more Ta than Cu ($N_{Cu-Cu/Ta} \approx 0.4/5.6$). This finding demonstrate a tendency for chemical order in the neighbour distribution that favors the hetero-atomic correlation as opposed to a random distribution, as evident in the Fig.2. This result indicates a reduced num-

ber of Cu–O–Cu dimers (Cu :: Cu) in the structure compared with dimers where one Ta atoms lie between the Cu atoms, i.e., Cu :: Cu \equiv Cu–O–Ta–O–Cu. Noticeably, because the likelihood of finding either Cu or Ta around Ta is approximately 50%, the probability of forming Cu dimers with more than one intervening Ta atom declines rapidly.

We now relate these findings to the observed magnetic behavior of BCTO. The temperature dependence of magnetic susceptibility (χ) is shown in Fig. 3(a). No signs of magnetic ordering could be seen at any temperature above 3 K (the lowest temperature in our experiment). The zero-field-cooled (ZFC) and field-cooled (FC) plots overlap indicating the absence of any spin-glass-like phase due to randomness. The Curie-Weiss fit gives an effective moment of $\mu_{\text{eff}} = 1.85 \pm 0.05 \mu_B$, in good accord with Cu²⁺ (spin 1/2), and $\theta_{\text{CW}} = -35 \pm 10$ K. As shown in Fig. 3(c)[inset] $\chi(T)$ exhibits an approximate $T^{-0.67}$ divergence down to about 4 K, below which a slight deviation is seen. The main panel shows an approximate data collapse at low temperatures when $(\mu_0 H)^{0.67} \chi$ is plotted against $T/\mu_0 H$. Similarly, M(H) plots at various temperatures between 3 K and 9 K, shown in Fig. 3(b), exhibit

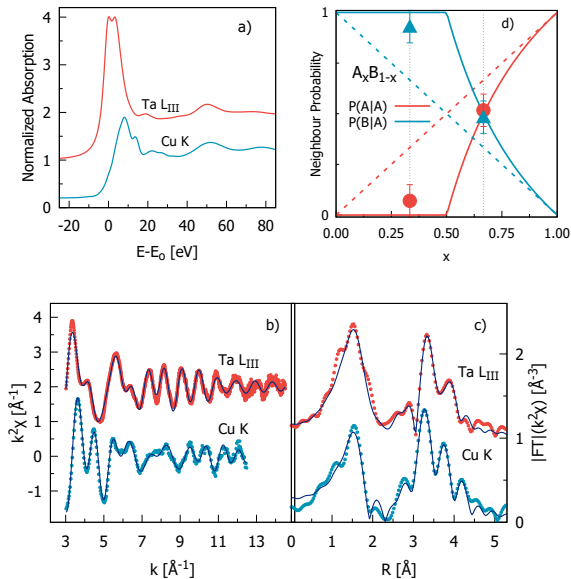


FIG. 2. (a) Normalized Ta-LIII and Cu-K edge XANES spectra, with the energy scale given relative to the edge energy ($E - E_0$) to facilitate comparison; (b) k^2 -weighted experimental EXAFS data (dots) and corresponding best-fit curves (solid lines) at the Cu and Ta edges for the BCTO sample; (c) moduli of the k^2 -weighted $|FT|$ of the experimental data (dots) and best fit curves (solid lines) for the various spectra; the curves are vertically offset for clarity. (d) homo-atomic (red) and hetero-atomic (blue) neighbour probabilities around the absorber plotted as a function of absorber concentration x , for both random distribution (dashed lines) and chemical order (solid lines) models (see text), compared with the experimental data, where $x = 0.33$ (0.66) corresponds to the Cu (Ta) edge results.

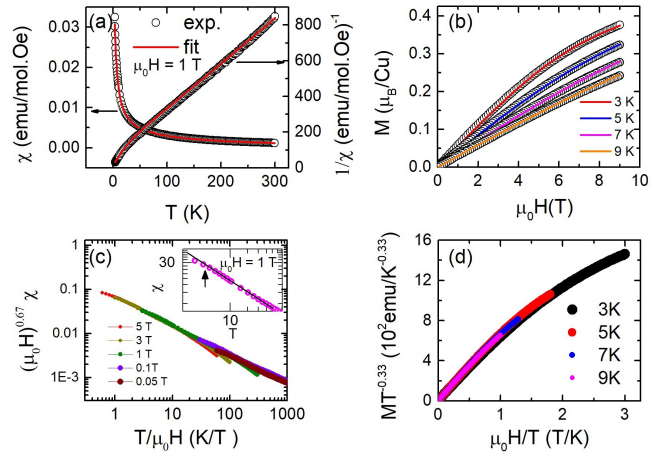


FIG. 3. (a) Magnetic susceptibility χ and χ^{-1} plotted as a function of temperature; (b) isothermal magnetization $M(H)$ at various temperatures. The solid lines in (a) and (b) are fits to the data (see text); (c) and (d) show data scaling behavior for $\chi(T)$ and $M(H)$, respectively. Inset in (c) shows $\chi(T)$ on a double-log plot. The units are same as in (a). The arrow indicates departure from $T^{-\gamma}$ at low temperatures.

the $M[H, T]$ -scaling, as shown in Fig. 3(d).

The specific heat, plotted as c_p/T for $\mu_0 H = \{0, 3, 5, 7, \text{ and } 9 \text{ T}\}$, is shown in Fig. 4(a). It exhibits a Schottky peak at low temperatures: the peak broadens and shifts to higher temperatures with increasing H . The very low temperature upturn is attributed to the onset of nuclear Schottky contribution. The c_{mag}/T is plotted in Fig. 4(d). The magnetic entropy ΔS_{mag} , estimated by integrating c_{mag}/T above 0.1 K, is shown in Fig. 4(d) (inset). c_{mag} is obtained by subtracting the phonon part (c_{ph}) from c_p (see Ref. [15]). ΔS_{mag} saturates at a value of $\approx 0.4 \ln R$ near 20 K. This suggests a significant zero-point entropy with almost as many as 60% of the Cu spins remaining dynamic down to temperatures as low as 0.1 K.

In the random-singlet phase c_{mag} is expected to diverge as $T^{1-\gamma}$ ($\gamma = 0.67$ in accordance with the χ and $M[H, T]$ -scaling). However, the c_{mag} data below 1 K follows a T-linear behavior, as shown in the inset of Fig. 4(b), which deviates significantly from the expected $T^{0.33}$ form. Furthermore, $(\mu_0 H)^\gamma c_p/T$ versus $T/\mu_0 H$ plots do not show the expected data collapse for $\gamma = 0.67$ (or any other γ value Ref. [15], as shown in Fig. 4(b)). There is an approximate convergence in the narrow range: $0.3 < T/\mu_0 H < 1$ or $0.9 \text{ K} < T < 3 \text{ K}$, but the low temperature deviation is significant.

In frustrated spin systems with quenched disorder, while the frustration prevents long-range ordering, the quenched disorder causes a small fraction of spins, positioned randomly due to disorder, to form the RS ground state, with the distribution of J 's often given by $P(J) \propto J^{-\gamma}$. As a result, the thermodynamics properties at low temperatures are dominated by these weakly coupled dimers, resulting in power-law and data-scaling behav-

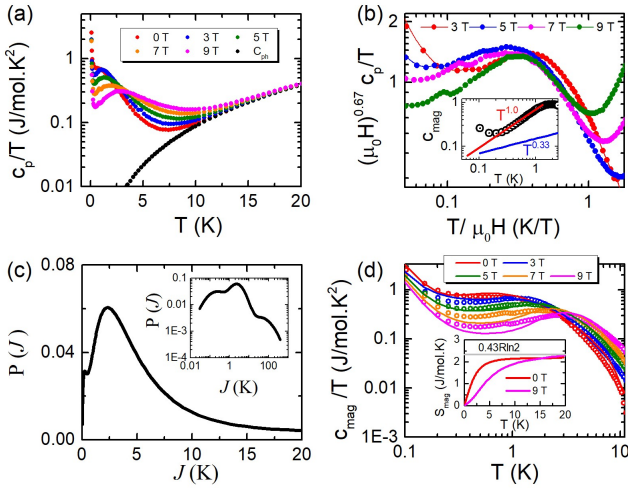


FIG. 4. (a) The temperature variation of specific heat plotted as c_p/T (phonon contribution is also shown); (b) $(\mu_0 H)^{\gamma} c_p/T$ ($\gamma = 0.67$) plots against $T/\mu_0 H$ for various applied fields are shown not to obey the scaling behavior. Inset in (b) shows c_{mag} varying linearly with T (red line). $T^{0.33}$ (blue line) is also shown to emphasize non-compliance with the random-singlet ground state; (c) exchange-coupling distribution $P(J)$ obtained here (inset: double-logarithmic plot of the same); (d) $c_{\text{mag}}(T)/T$ versus T plots for various H . The solid lines in (d) are fit to the data (inset shows the temperature variation of S_{mag} for $\mu_0 H = 0, 9$ T).

ions. On the other hand, in BCTO with high-density of spin-1/2's placed randomly on a pseudo-cubic lattice, the expected behavior is not seen at very low temperatures.

We thus develop a unified distributed-exchange dimer model, which makes no *a priori* assumption on the form of $P(J)$. Instead, $P(J)$ is reconstructed from the experimental data as explained here. For numerical flexibility, we represent $P(J)$ as a sum of log-normal components:

$$P(J) = \sum_{k=1}^K w_k \frac{1}{J \sigma_k \sqrt{2\pi}} \exp \left[-\frac{(\ln J - \ln J_{0k})^2}{2\sigma_k^2} \right], \sum_k w_k = 1. \quad (1)$$

Here, J_{0k} and σ_k are the median and width of each component, and w_k its normalized weight. This flexible yet compact form allows $P(J)$ to capture both narrow and broad features, enabling a direct reconstruction from the data without imposing a theoretical bias. Further details are provided in the Supplementary Material [15].

The model includes: (i) antiferromagnetic spin-1/2 dimers obeying $P(J)$ in eq. 1, and (ii) a small fraction, f , of paramagnetic monomers (orphan spins). The expressions for $\chi(T)$, $M(H, T)$, and $c_{\text{mag}}(H, T)$ are given in the Supplementary Material [15]. All datasets, $c_{\text{mag}}(T, H)$, $\chi(T)$, and $M(H, T)$, were fitted simultaneously using a global least-squares objective. The best-fit solution reproduces all datasets with an average normalized root-mean-square deviation of approximately 3%, as shown in figure 3(a), (b), and 4(d), respectively. The monomer fraction obtained is $f \simeq 0.04$.

The reconstructed $P(J)$, shown in Fig. 4, is very broad, spanning over two decades in energy, and characterized by a broad peak at $J \approx 4$ K with shoulder-like features at 70 K and 0.1 K, and with a long but non-diverging low- J tail. As discussed before, the Ta-rich local environment around Cu suppresses direct Cu-O-Cu type dimers compared to the dimers formed with at one intervening Ta. Similarly, the near-equal Cu/Ta coordination around Ta, sharply reduces the number of intervening Ta. Accordingly, we ascribe the high-temperature feature near 70 K to the Cu-O-Cu superexchange. This is consistent with the Weiss temperature θ_{CW} , and the value of J for related perovskite cuprates [21]). The observed decrease by an order of magnitude with an additional Ta atom in the exchange path (4 K peak) is also reasonable, as is the further reduction by another order of magnitude with two or more intervening Ta atoms (0.1 K feature and low- J tail). That the number density of dimers with one intervening Ta is significantly larger is also in qualitative agreement with the distribution of Cu and Ta.

The additional broadening of these features arises from the strong dependence of effective exchange couplings on cluster geometry, as confirmed by Exact-Diagonalization calculations (see Supplementary Material [15]). Further, the primary J for $P4/mmm$ and $P4mm$ differ slightly, the B-O-B bond angle being 180° and 169° , respectively.

Incidentally, above the $J/k_B = 4$ K, the $P(J)$ versus J plot has an approximate power-law behavior. This becomes more evident in the log-log plot shown in the inset of Fig. 4, which reveals an approximate linear regime above 4 K, inclined at a slope of ≈ -0.7 . Therefore, on the high-temperature side of the 4 K peak, $P(J)$ resembles a typical power-law dependence, which may account for the apparent power-law and scaling behavior seen in our data above 3 K, but not at the low temperatures.

To summarize, we studied the disordered perovskite BCTO, where Cu and Ta randomly occupy a pseudo-cubic B-sublattice. The nature of this disorder was characterized using EXAFS. We find no evidence for long-range magnetic order or spin freezing down to 0.1 K. The magnetic ground state is best described as a collection of singlets with a broad but non-singular distribution $P(J)$ of exchange couplings, consistent with the structurally constrained exchange paths inferred from EXAFS data. Our results point to a class of three-dimensional spin-disordered materials in which disorder leads to broad, but finite, exchange distributions and does not drive the system toward an infinite-randomness fixed point.

ACKNOWLEDGMENTS

Portions of this research were carried out at the light source PETRA-III of DESY, a member of the Helmholtz Association (HGF). We would like to thank the beamline scientists for assistance at the beamlines P65 and

P02.1. Financial support by the Department of Science & Technology (Government of India) provided within the framework of the India@DESY collaboration is gratefully acknowledged. SM would like to acknowledge the University Grants Commission (UGC), India, for financial support in the form of a research fellowship. SM is also grateful to the I-HUB Quantum Technology Foundation (QTF) at IISER, Pune, for financial support under the Senior Research Fellowship scheme. SM acknowledges Dr V.S. Patankar Dissertation Fellowship for supporting through a one-time financial aid.

APPENDIX

I. EXAFS AND CHEMICAL ORDERING

To understand how EXAFS analysis can deduce the local chemical order in binary alloys, that is the relative arrangement of neighboring species, let us consider a solid solution made of two atomic species, A and B , randomly occupying the sites of a cubic lattice with composition $A_x B_{1-x}$. Different situations may arise. For a perfectly random distribution (R), the probability of finding a pair of neighboring atoms is determined solely by the relative concentrations of the two species. Thus, the probabilities of finding AA , BB , and AB pairs are, respectively,:

$$P_R(AA) = x^2, \quad P_R(BB) = (1-x)^2, \quad P_R(AB) = 2x(1-x).$$

Alternatively, the system may exhibit a preference for either *hetero-atomic* or *homo-atomic* coordination. If hetero-atomic coordination is preferred (chemically ordered arrangement, CO), the number of AB pairs is maximized, so for $x < 0.5$, $P_{CO}(AA) = 0$ and the other probabilities are:

$$P_{CO}(AB) = 2x, \quad P_{CO}(BB) = 1 - P_{CO}(AB),$$

while for $x \geq 0.5$ $P_{CO}(BB) = 0$ the relations are:

$$P_{CO}(AB) = 2(1-x), \quad P_{CO}(AA) = 2x - 1$$

In the case of homo-atomic preference(H), the probabilities become

$$P_H(AA) = x, \quad P_H(BB) = 1 - x,$$

which corresponds to phase separation into A -rich and B -rich regions. Let us now fix A as the absorber and x the absorber concentration. Since XAFS is chemically selective, it probes the conditional probability of finding a specific neighboring species given the absorber A . This is obtained by dividing the probability of the pair by the absorber concentration. In the case of a random distribution, the conditional probabilities are

$$P_R(A|A) = x, \quad P_R(B|A) = 1 - x.$$

In the chemically ordered model, B neighbors are maximized so for $x \leq 0.5$, we obtain

$$P_{CO}(B|A) = 1, \quad P_{CO}(A|A) = 0,$$

while for $x \geq 0.5$, the conditional probabilities are:

$$P_{CO}(B|A) = \frac{1}{x} - 1, \quad P_{CO}(A|A) = 2 - \frac{1}{x}.$$

In the BCTO EXAFS analysis, the multiplicity of Cu-Cu/Ta (and Ta-Ta/Cu) neighbors along the pseudo-cube is refined by constraining the total coordination number to 6 and weighted by the homo-atomic ($y = P(A|A)$) and hetero-atomic ($1 - y = P(B|A)$) pair probabilities. The experimental results at the Cu and Ta edges are shown in Fig.2d. It is evident that, although the results carry a certain degree of uncertainty due to the complexity of the analysis and the difficulty of disentangling the different contributions, the experimental data suggest a clear tendency towards a hetero-atomic correlations and are consistently reproduced at both absorption edges. Such a preference for hetero-atomic correlation is not unexpected, as alternating Cu and Ta on the lattice reduces strain energy arising from the different shapes and sizes of the CuO_6 and TaO_6 octahedra.

[1] C. Dasgupta and S. K. Ma, Low-temperature properties of the random heisenberg antiferromagnetic chain, *Phys. Rev. B* **22**, 1305 (1980).

[2] S. K. Ma, C. Dasgupta, and C. K. Hu, Random antiferromagnetic chain, *Physical review letters* **43**, 1434 (1979).

[3] D. S. Fisher, Random antiferromagnetic quantum spin chains, *Physical Review B* **50**, 3799 (1994).

[4] I. Kimchi, A. Nahum, and T. Senthil, Valence bonds in random quantum magnets: Theory and application to YbMgGaO_4 , *Phys. Rev. X* **8**, 031028 (2018).

[5] J. P. Sheckleton, J. R. Neilson, D. G. Soltan, and T. M. McQueen, Possible valence-bond condensation in the frustrated cluster magnet $\text{LiZn}_2\text{Mo}_3\text{O}_8$, *Nature materials* **11**, 493 (2012).

[6] I. Kimchi, J. P. Sheckleton, T. M. McQueen, and P. A. Lee, Scaling and data collapse from local moments in frustrated disordered quantum spin systems, *Nature communications* **9**, 4367 (2018).

[7] Z. Zhu, P. Maksimov, S. R. White, and A. Chernyshev, Disorder-induced mimicry of a spin liquid in YbMgGaO_4 , *Physical review Letters* **119**, 157201 (2017).

[8] Z. Ma, J. Wang, Z.-Y. Dong, J. Zhang, S. Li, S.-H. Zheng, Y. Yu, W. Wang, L. Che, K. Ran, *et al.*, Spin-glass ground state in a triangular-lattice compound YbZn_2

GaO₄, Physical Review Letters **120**, 087201 (2018).

[9] S. Kundu, A. Hossain, R. Das, M. Baenitz, P. J. Baker, J.-C. Orain, D. Joshi, R. Mathieu, P. Mahadevan, S. Pu-jari, *et al.*, Signatures of a spin-1/2 cooperative paramagnet in the diluted triangular lattice of Y₂CuTiO₆, Physical review letters **125**, 117206 (2020).

[10] P. Song, K. Zhu, F. Yang, Y. Wei, L. Zhang, H. Yang, X.-L. Sheng, Y. Qi, J. Ni, S. Li, Y. Li, G. Cao, Z. Y. Meng, W. Li, Y. Shi, and S. Li, Evidence for the random singlet phase in the honeycomb iridate SrIr₂O₆, Phys. Rev. B **103**, L241114 (2021).

[11] M. A. de Vries, A. McLaughlin, and J.-W. Bos, Valence bond glass on an fcc lattice in the double perovskite Ba₂YMoO₆, Physical review letters **104**, 177202 (2010).

[12] S. Hossain, S. Rahaman, H. Gujrati, D. Bhoi, A. Matsuo, K. Kindo, M. Kumar, and M. Majumder, Evidence of random spin-singlet state in the three-dimensional quantum spin liquid candidate Sr₃CuNb₂O₉, Physical Review B **110**, L020406 (2024).

[13] B. Sana, M. Barik, S. Lee, U. Jena, M. Baenitz, J. Sichelschmidt, S. Luther, H. Kühne, K. Sethupathi, M. R. Rao, *et al.*, Possible realization of a randomness-driven quantum disordered state in the S = 1/2 antiferromagnet Sr₃CuTa₂O₉, Physical Review B **110**, 134412 (2024).

[14] B. R. Coles, B. V. B. Sarkissian, and R. H. T. and, The role of finite magnetic clusters in au-fe alloys near the percolation concentration, Philosophical Magazine B **37**, 489 (1978).

[15] S. M. et al., Exploring the random-single ground state in disordered perovskites, Supplementary Material (2025).

[16] H. Asakura, T. Shishido, S. Yamazoe, K. Teramura, and T. Tanaka, Structural analysis of group v, vi, and vii metal compounds by xafs, J. Phys. Chem. C **115**, 23653 (2011).

[17] C. Meneghini, F. Bardelli, and S. Mobilio, Estra-fitexa: a software package for exafs data analysis, Nuclear Instruments and Methods in Physics Research Section B: Beam Interactions with Materials and Atoms **285**, 153 (2012).

[18] J. Boyce and J. Mikkelsen, Local structure of pseudobinary semiconductor alloys: An x-ray absorption fine structure study, Journal of Crystal Growth **98**, 37 (1989).

[19] C. Meneghini, F. Boscherini, F. Evangelisti, and S. Mobilio, Structure of α -Si_{1-x}C_x: H alloys by wide-angle x-ray scattering: Detailed determination of first-and second-shell environment for si and c atoms, Physical Review B **50**, 11535 (1994).

[20] C. Meneghini, S. Ray, F. Liscio, F. Bardelli, S. Mobilio, and D. D. Sarma, Nature of “disorder” in the ordered double perovskite Sr₂FeMoO₆, Phys. Rev. Lett. **103**, 046403 (2009).

[21] H. D. Zhou, E. S. Choi, G. Li, L. Balicas, C. R. Wiebe, Y. Qiu, J. R. D. Copley, and J. S. Gardner, Spin liquid state in the S = 1/2 triangular lattice Ba₃CuSb₂O₉, Phys. Rev. Lett. **106**, 147204 (2011).